Available online at www.sciencedirect.com
SCIENCE DIRECT
ELSEVIER
Polymer Testing 25 (2006) 460–469
POLYMER TESTING
www.elsevier.com/locate/polytest

Material Behaviour

Influence of flow on the global crystallization kinetics of iso-tactic polypropylene

A. Godara[a], D. Raabe[a,*], P. Van Puyvelde[b], P. Moldenaers[b]

[a]*Max-Planck-Insitut fur Eisenforschung, Max-Planck-Str. 1, 40237 Düsseldorf, Germany*
[b]*Department of Chemical Engineering, Katholieke Universiteit Leuven, Belgium*

Received 9 December 2005; accepted 25 January 2006

Abstract

The crystallization behavior of iso-tactic polypropylene (iPP) has been studied placing particular emphasis on the influence of flow on the global kinetics of crystallization. In order to quantify the kinetics an Avrami-type approach has been used. The results are discussed in the context of the Doi–Edwards independent alignment approximation (DE-IAA) model for flow-induced crystallization.

Keywords: iPP; Crystallization; Flow; Avrami; Induction time; DE-IAA model

1. Introduction

The study of polymer melt crystallization stimulated by flow has attracted much interest because it implies the possibility of controlling the final morphology and the resulting mechanical and functional properties of semi-crystalline polymers [1]. By changing the processing conditions (temperature, strain) and molecular composition, a wide range of molecular morphologies, such as spherulites, shish-kebab or row-nucleated structures can be produced which opens up the possibility of tailoring desired microstructures. Flow-induced orientation and structure formation in elongation flow were thoroughly studied by Keller and co-workers [2]. Also, for the case of crystallization under quiescent conditions, the mechanism of crystal growth from the melt has become a subject of increasing attention [3–5].

Experiments that monitor the earliest stages of flow-enhanced crystallization of semi-crystalline polymers provide valuable clues regarding the microscopic origin of the effects of flow on the overall crystallization kinetics and morphology observed during and after flow. An improved understanding of the fundamentals of flow-enhanced crystallization effects can help to tailor advanced processing strategies which are guided by a better insight into the interplay between macromolecular flow dynamics and polymer crystallization.

Obtaining a complete understanding of the fundamentals of structure development during processing from a molecular perspective, which would help to explain the effect of changing resin composition (polymer characteristics and/or

*Corresponding author. Tel.: +49 211 6792278; fax: +49 211 6792333.
E-mail address: raabe@mpie.de (D. Raabe).

0142-9418/$ - see front matter © 2006 Elsevier Ltd. All rights reserved.
doi:10.1016/j.polymertesting.2006.01.010

additives) or processing variables on specific material properties, remains a challenge (see e.g. [6–12]). Most experiments that examine row-nucleated structures mimic the high strain and shear rates typical of polymer processing operations, but the complicated thermal and flow history experienced by a polymer make it difficult to infer the molecular variables that control the semi-crystalline morphology that develops.

In this work, the effect of an imposed shear flow on the morphology and the kinetics of isothermal crystallization of an iPP has been studied experimentally. The different factors that may contribute to flow-enhanced crystallization have been varied systematically. The magnitude of the shear rate, the shearing time, as well as the instant in time at which the deformation starts, have all been varied in combination with a well-defined flow field and the use of rheo-optical measurements. The focus of previous works in this field was placed essentially on the investigation of the overall global kinetics [13–15] and the changes in the induction times during isothermal crystallization [13,16]. It has been shown that both factors are considerably enhanced by flow. It has been suggested that the main effect of flow on these changes is the modification of the nucleation process and the resulting change in the nucleation density. Under certain conditions, however, even the morphologies will change as a consequence of the experienced flow-induced deformations. This effect occurs in the form of the change of the typical spherulite shape encountered under quiescent conditions to oriented crystallite structures, such as shish-kebab or row-nucleated structures [17]. Additionally, it has been shown that flow can also affect crystal growth kinetics [15,18]. Therefore, the kinetics of flow-induced crystallization is also studied in this work by means of the Avrami–Johnson–Mehl–Kolmogorov (AJMK) and the Doi–Edwards independent alignment approximation (DE-IAA) models in the framework suggested by Coppola et al. [19].

2. Theory

2.1. AJMK model

In order to quantify the kinetics of the crystallization process, an AJMK has been applied for data analysis, Fig. 3. The mathematical treatment of sphere growth leads to the well-known Avrami equation [20]:

$$\alpha(t) = 1 - \exp\left(-kt^N\right) = 1 - \alpha_a(t), \quad (1)$$

where $\alpha(t)$ is the crystalline volume fraction developed at time t, $\alpha_a(t)$ is the volume fraction of amorphous fraction at time t, k is the shape-dependent Avrami rate constant and N is the Avrami exponent.

The AJMK analysis considers the competitive isotropic growth of rigid spheres in space without making any special assumption about the inner structure of those spheres. In the current case, these growing spheres are the spherulites which are not completely crystalline [21–23], but they are two-phase composites consisting of crystalline and amorphous material.

2.2. DE-IAA model for the description of flow-induced crystallization

The last few years have seen significant progress in the development of constitutive relations for the description of polymer melt behavior and enhancement of global crystallization of kinetics under flow of polymeric systems. The latest of these is the DE-IAA proposed by Coppola et al. [19]. In their model, the crystallization kinetics is described in terms of an induction time. The basis of the approach is the calculation of the free energy change of a polymer chain during flow in terms of the Doi–Edwards theory using the independent alignment approximation. The assumptions for the model are:

1. The chain orientation accounts for the enhancement of crystallization at low deformation rates causing the free energy change.
2. An independent alignment approximation is adopted assumed to generate only minor deviation from the rigorous model in steady flow. [24,25].

In most polymer flow induced crystallization (FIC) experiments, a characteristic time for the onset of crystallization is measured. In isothermal experiments at an imposed shear rate, the time corresponding to a sudden upturn of the shear viscosity is considered as an induction time [26–32]. This induction time is roughly proportional to the inverse of the nucleation rate. For this reason, to estimate the effect of flow on crystallization, it is useful to introduce the ratio Θ between the

nucleation rate under flow and that under quiescent conditions, as a dimensionless induction time:

$$\Theta = \frac{\text{flow}}{\text{quiescent condition}}. \quad (2)$$

The DE-IAA model assumes that the primary effect of the flow acts on the nucleation process and does so in an additive way. The free energy for the quiescent crystallization can be expressed to a good approximation as

$$\Delta G_q = \Delta H_0 \left(1 - \frac{T_c}{T_m}\right), \quad (3)$$

where ΔG_q is the quiescent free energy change at the crystallization temperature T_c, T_m is the thermodynamic melting temperature and ΔH_0 is the change in latent heat of fusion. The effect of flow in terms of an increase of the nucleation rate can be expressed as a change in the free energy of the melt according to

$$\Delta G = \Delta G_q + \Delta G_f, \quad (4)$$

where ΔG is the free energy change of the melt and ΔG_f is the flow-induced free energy change of the melt phase. The explicit expression for ΔG_f derived from the micro-rheological model of Doi–Edwards is given in Ref. [33].

Based on the above-mentioned assumptions, the final equation to calculate a dimensionless induction time under the influence of flow is given by

$$\begin{aligned}\Theta &= \frac{\dot{N}_q}{\dot{N}_f} \\ &= \frac{1}{1 + (\Delta G_f/\Delta G_q)} \\ &\quad \times \exp\left(\frac{K_n}{T(\Delta G_q)^n}\left(\frac{1}{(1 + \Delta G_f/\Delta G_q)^n} - 1\right)\right) \\ &\cong \frac{\vartheta_f}{\vartheta_q}, \end{aligned} \quad (5)$$

where T is the absolute temperature, $\dot{N}$ the nucleation rate, K_n a constant and 'n' an exponent which also appears as a subscript for K and which accounts for the temperature region where the homogenous nucleation takes place. It can generally assume the values 1 and 2 [28]. ϑ is the induction time, the subscripts 'q' and 'f' stand for quiescent and flow conditions, respectively.

The model parameters required under isothermal conditions are the latent heat of fusion ΔH_0, the thermodynamic melting temperature T_m, the constant K_n, the characteristic model relaxation time, the constant polymer density and the molecular weight between the entanglements, M_e.

A summary of the experimentally determined parameters by Refs. [24–27] for each set of data used in the comparison is reported in Table 2. In our case, K_n is obtained by extrapolation to the melting temperature of our sample material isotactic polypropylene (iPP). Density and time of relaxation are used as reported by Devaux [34].

3. Experimental

3.1. Material

As starting materials, we used homopolymer iPP pellets which were supplied by AtoFina ($\bar{M}_w = 305,500$, $\bar{M}_n = 61,800$, isotacticity 95%). A wide distribution of macromolecular chain lengths ($I_p = \bar{M}_w/\bar{M}_n = 4.95$) and a rather high molecular weight were selected as strong effects of flow on crystallization can be anticipated for such materials [35].

3.2. Experimental set-up for light microscopy

A Linkam shearing cell CSS450 coupled with a Leitz polarized microscope has been used as a heating and shearing device for the experiments. The two parallel plates of the Linkam cell were temperature controlled using two electrically driven heating elements. The observation zone was located in the middle of the radius of the upper plate. Although the global flow is non-homogenous, this is not a serious drawback as the observation zone is small and, hence, the local shear rate can be assumed to be constant. A Pulnix CCD camera has been used to capture and to digitize the pictures of the crystallizing sample.

3.3. Rheology

The rheological behavior of iPP was measured by a dynamic stress rheometer (DSR) using parallel plate geometry. Sample disks were cut from the sheet of iPP to fit the 25 mm diameter of the parallel plates. After mounting the sheets into the DSR device, the sample was heated to the initial temperature of $T_m = 483$ K under N_2 atmosphere. As soon as the melt occurred, the gap between the plates was adjusted to 0.339 mm and the excess material was scraped from the sides of the plates, which resulted in samples with a diameter of 25 mm. The samples were kept at the melting temperature

T_m for 15 min in order to erase memory effects stemming from previous treatments. After that, the temperature was lowered at a rate of 10 K/min down to the crystallization temperature of 409 K. The storage modulus, loss modulus and complex viscosity were measured in a nitrogen environment. The properties were measured in the dynamic mode with an oscillation frequency of 1 rad/s. The moment at which the melt reached the crystallization temperature, the shear rate was applied for 60 s. The instant at which the deformation finished, the representative time started. The storage and loss moduli, G' and G'', and the tangent of the loss angle, $\tan\delta$, were measured against the time scale. For clarity in the present case we plot only the loss modulus.

3.4. Thermo-mechanical protocol

The thermo-mechanical protocol used for the crystallization experiments is described in Fig. 1. Polymer films with a thickness of 500 μm were prepared by pressing pellets at $T = 483$ K for 5 min. Disks were cut from these films. They were inserted into the Linkam cell and heated up to the melting point of $T_m = 483$ K. Their thickness was fixed to 300 μm by slowly lowering the upper glass plate of the Linkam device. Subsequently, the sample was kept under these conditions at the melting point for 5 min. From the relaxation spectrum, the relaxation time calculated was 10 s and, accordingly, the samples were kept in the melt at 483 K [34]. Athermal nuclei might still be present, as suggested by Alfonso and Ziabicki [36], but as all the parameters are kept constant, mechanical effects were assumed to have relaxed as the sample was held for several times the longest relaxation time in the melt.

After this treatment, the sample was cooled at a fixed cooling rate, until the desired respective crystallization temperature was reached. During cooling (cooling rate was always 10 K/min), the gap was finally adjusted to 285 μm in order to compensate for the volumetric shrinkage of the sample that can cause slip during shear or bubble formation. From pVT (pressure–volume–temperature) measurements, the volumetric shrinkage was estimated as 5 vol% during cooling. During isothermal crystallization, two times were defined to describe the shear experiment, Fig. 1.

A commonly used approach to evaluate the effect of shear flow is to start the flow immediately after isothermal conditions are reached ($t_0 = 0$). When experiments at different strains are compared, the

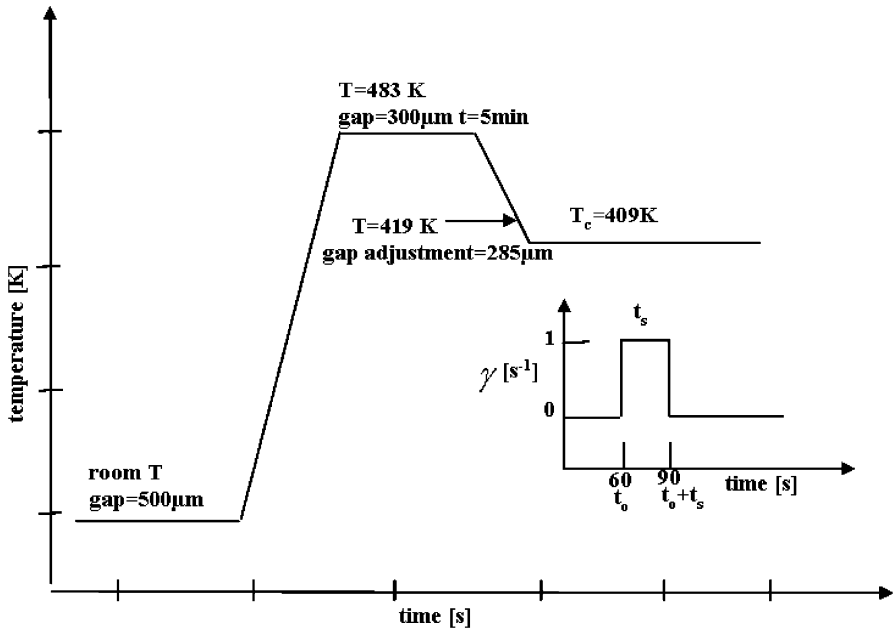

Fig. 1. Experimental thermo-mechanical protocol showing the flow induced crystallization experiment with the thermal and the flow history used for the iPP, $T_c = 409$ K, shear rate 1/s, time of shearing $t_s = 30$ s and time of induction of shearing $t_0 = 60$ s. Where t_0: time elapsed between the beginning of isothermal conditions and the inception of the shear flow, i.e. t_0 represents that instant of time during which the flow is applied and t_s: duration of the application of shear.

moment at which flow is stopped will obviously vary. One specific aim of the present experiments is to verify whether there is an effect of the instant in time at which the flows are applied and stopped. As the structure is continuously evolving during crystallization, this cannot be ruled out a priori. Therefore, different experimental protocols were used to observe the effect of different parameters shearing rate, shearing time, and the instant in time at which the deformation starts under a well defined flow field.

4. Results and discussion

4.1. Quiescent crystallization

In order to obtain a reference state for the flow experiments, quiescent crystallization experiments were also performed. We evaluated the morphology and the spherulite growth rate G (μm/min) by measuring the average spherulite size versus time under similar isothermal conditions following the same thermo mechanical protocol.

Fig. 2 shows the developed spherulitic morphology. In Table 1 the results are compared with literature results obtained by other groups. Our results are in good agreement for the same values of T_c and also coherent with the decrease in growth rate at higher T_c observed earlier by other groups. The variation of the growth rates at similar crystallization temperature can be explained by the difference in molecular weight and the tacticity of the material (see Kolb et al. in Ref. [37]).

The AJMK analysis applies well to the current case since spherulites indeed tend to grow as isotropic spheres at the initial and intermediate stages of crystallization. However, at the late stages of crystallization the application of the AJMK approach becomes less trivial since the spherulite sizes are becoming comparable to the gap between the parallel plates of the Linkam cell (the mutual impingement of the spherulites is statistically accounted for by the AJMK model).

The Avrami exponent N found by analyzing the data presented in Fig. 3b amounts to 2.7, which is close to the value of 3, indicating instantaneous and site-saturated nucleation conditions as well as isotropic 3D growth behavior of the spherulites. This is coherent with the observed small size distribution of the spherulites. The data found in this study are in close agreement with the values reported by Devaux ($N = 2.5$), which were determined under the same thermal conditions using the DSC method. This value is small compared to the theoretical predictions of the Avrami model for isotropic spherulites (between 3 and 4 depending on nucleation conditions), but similar values are reported for instantaneous site-saturated nucleation conditions for the crystallization of polypropylene by Devaux in Refs. [38,39]. The kinetics are characterized in terms of the Avrami rate constant k, which is related to the growth rate and to the number of activated nuclei. Here the value of k is found to be $5.82 \times 10^{-11}\,s^{-3}$.

4.2. Crystallization under flow

4.2.1. Effect of shear rate

Figs. 2b–d show the effect of different shear rates on the morphology of the spherulitic structure during crystallization at $T_c = 409\,K$. The experiments were performed at a shearing time $t_s = 30\,s$ and a induction time $t_0 = 0$. The applied shear rates were all in the onset of the shear-thinning regime. The first effect arising from the applied shear is the increase in the nucleation density. This effect leads to a decrease in the final average spherulite size, which is in good agreement with earlier results reported by various groups in the literature [38,40].

Fig. 4 shows the corresponding Avrami analysis. Fig. 4b shows the expected increase in the Avrami rate constant as a function of the shear rate. The change in the Avrami constant k as a function of the imposed shear can be described by $k_{shear} = b\dot{\gamma}^a$, where a and b are fitted as 3.6 and 2.4, respectively. This indicates that a change of a factor of 2 in the imposed shear rate results in a ten-fold increase in the crystallization rate.

4.2.2. Effect of time of induction t_0

Figs. 2c and e show the effect of the induction time t_0 on the development of the morphology. The experiments were performed at a constant shear rate of $1\,s^{-1}$ and constant shearing time of 30 s at an isothermal crystallization temperature of 409 K. As expected, from optical micrographs it is observed that an increase in time of induction of shear flow caused a drop in the density of nuclei [38], hence slowing down the overall kinetics and resulting in an increased average size of the spherulites.

The start of crystallization is observed even during the cooling trajectory [33], i.e. while the polymer melt is cooled down from a higher temperature to crystallization temperature. After

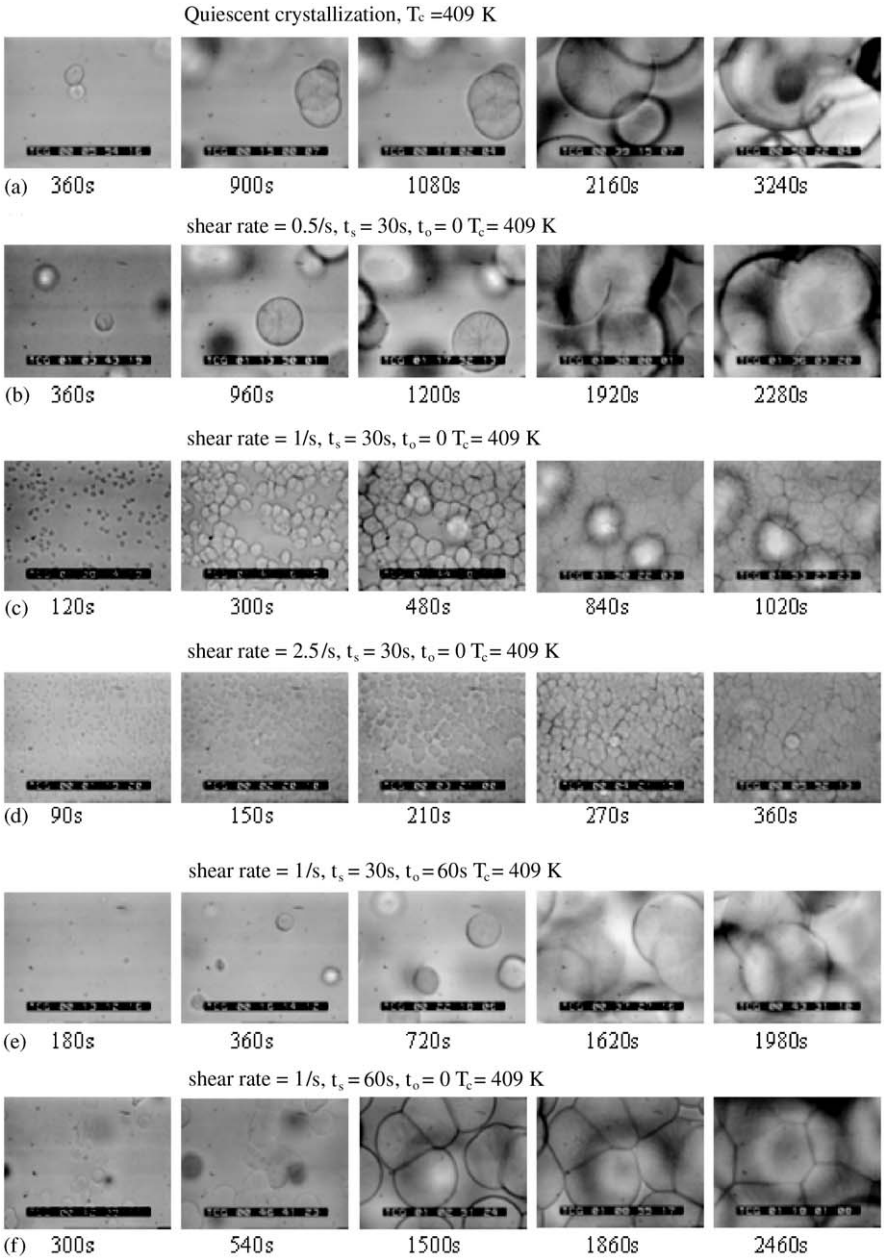

Fig. 2. Optical micrographs taken during the crystallization process after various quiescent and shear treatments (micrograph size: $240 \times 180\,\mu m^2$).

Table 1
Comparison of the growth rates as obtained by various research groups at 409 K and higher temperatures with various experimental techniques

Literature reference	Crystallization temperature T_c [K]	Growth rate [μm/min]	Final size (radius) [μm]	Techniques used for analysis
Kolb et al. [37]	421	1.50	80	Optical microscopy and X-ray
Devaux [34]	409	3.24	70	Optical microscopy
This study	409	3.61	74	Optical microscopy

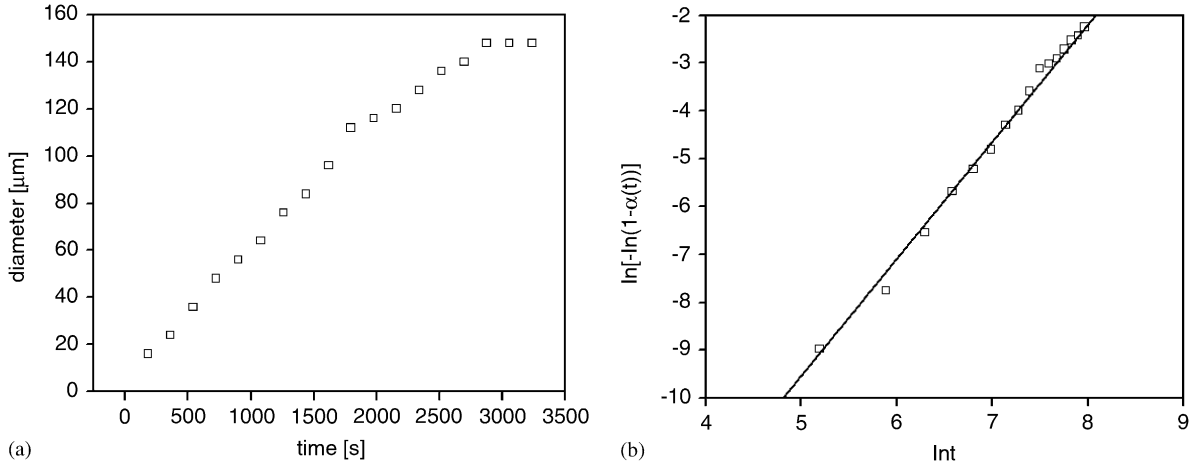

Fig. 3. (a) Quiescent crystallization of iPP at isothermal crystallization temperature 409 K. (b) Avrami analysis applied to the data shown in Fig. 3a.

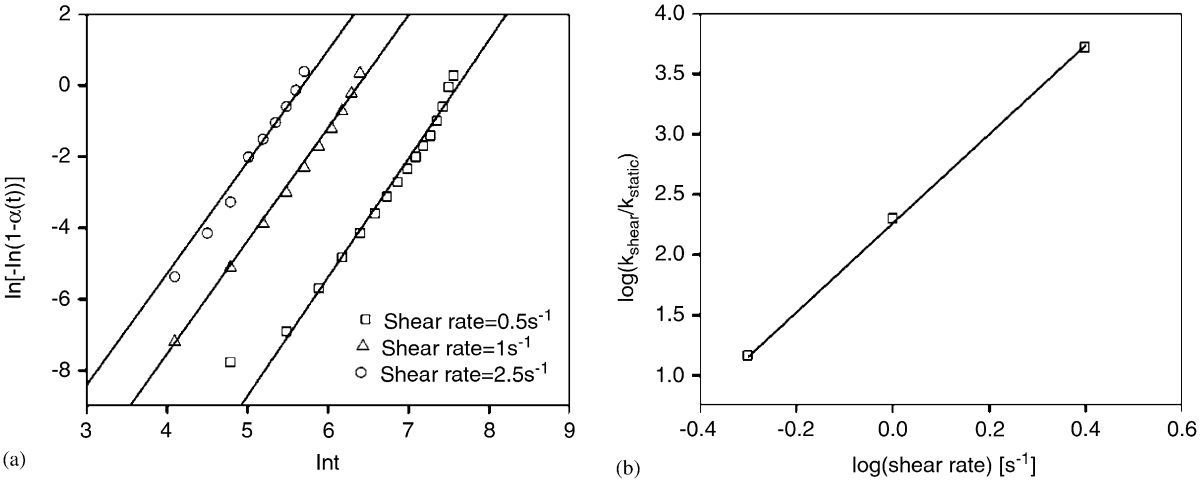

Fig. 4. Avrami analysis: (a) Effect of shear rate at constant shearing time ($t_s = 30$ s) and induction time ($t_0 = 0$). (b) Relationship between the kinetic rate constants, k_{shear}/k_{static}, as a function of the shear rate for iPP under isothermal conditions at $T_c = 409$ K.

reaching the crystallization temperature, the waiting time, i.e. the increased time of induction, t_0, gives more time for the crystallites to grow. Hence, applying shear at this stage will most likely affect the normal growth of the crystallites. Our results are in agreement with this observation. Fig. 5 shows the kinetic analysis which reveals that the Avrami rate constant has decreased from 4.05×10^{-9} to $2.17 \times 10^{-10}\,s^{-3}$ with an increase in the time of induction.

4.2.3. *Effect of shearing time t_s*

Figs. 2c and f show the effect of the shearing time on the morphology of growing spherulites. The experiments were performed at a constant shear rate of 1/s and at a constant time of induction, $t_0 = 0$ s. After shearing for a long time, the formation of row nuclei is observed. They form thread like precursors before appearing as independent nuclei in the melt. This phenomenon has already been observed by several other groups [17,41] and recently characterized by using WAXS and SAXS studies [2,7,11,42,43]. The second observation is a substantial decrease in nucleation density at higher shearing times which finally results in increased spherulite size. The earlier experimental observations have revealed that the formation of nuclei is a multi-step process [44,45]. The authors have shown the

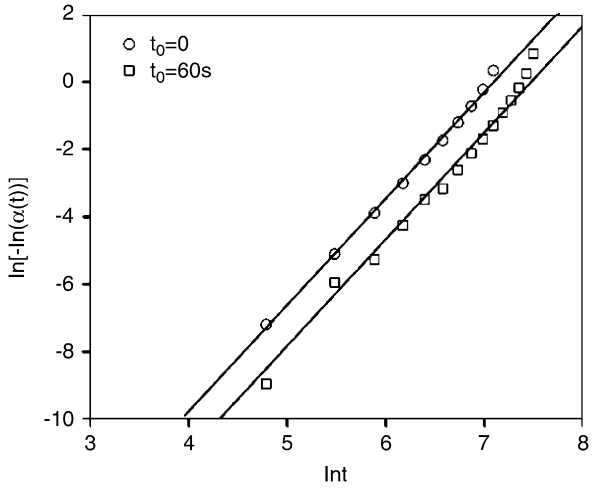

Fig. 5. Avrami analysis: effect of induction time (t_0) at constant shearing time ($t_s = 30$ s) and under a constant shear rate of $1\,s^{-1}$ during iPP crystallization at an isothermal crystallization temperature of $T_c = 409$ K.

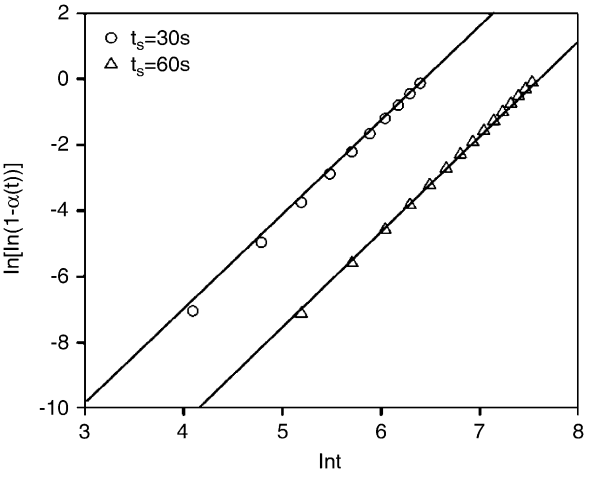

Fig. 6. Avrami analysis: effect of shearing time (t_s) at constant time of induction ($t_0 = 0$ s) and under a constant shear rate of $1\,s^{-1}$ during iPP crystallization at an isothermal crystallization temperature of $T_c = 409$ K.

formation of the localized dense entities with some preferable chain alignment, which acts as nuclei precursors.

This decrease in nucleation density can be explained by the coalescence of growing row nuclei at very early stages, i.e. before appearing as independent nuclei.

It is obvious that the growth rate will be affected if growing spherulites encounter obstacles that disturb their free growth in terms of some spatial system inhomogeneity [41]. The direct measurement of growth rates for such impinging spherulites is intricate. Hence, the overall kinetics of crystallization are expressed in terms of Avrami rate constant.

Fig. 6 shows an Avrami analysis revealing this effect. The Avrami rate constant k decreased from 4.05×10^{-9} to $2.27 \times 10^{-10}\,s^{-3}$ with an increase in the shearing time. This slowing down of the overall Avrami kinetics is coherent with our results of a drop in the nucleation density.

However, these results are not consistent with results reported by Devaux et al. [38] who observed in their work a power law behavior, i.e. the overall kinetics increased with an increase in the shearing time. A possible explanation for this contradiction to our results could be the cumulative effect of the shear rate and the shearing time. Devaux et al. [38] performed experiments at very low shear rates which does not affect the shape of growing crystallites even at longer shearing times.

Devaux et al. [38] introduced a parameter $t_{0,max}$ to describe the cumulative effect of the shear rate and shearing time on the kinetics of crystallization in terms of a critical dwell time. The author assumed that if the end of shearing occurs before some critical dwell time, $t_{0,max}$, there is no effect on crystallization. However, if the shearing was longer than $t_{0,max}$, the kinetics were assumed to be slowed down. According to this approach, one might conclude from our data that a higher shear rate decreases the critical dwell time, $t_{0,max}$. Indeed, our observations show the cumulative effect of the shear rate and the shearing time.

Fig. 7 shows the loss moduli obtained for the quiescent and for the shearing experiments. Fig. 7b reveals that even under isothermal conditions the origin of the G'' curves are different because the time scale was defined to start from the moment at which the deformation had ended, but the onset of crystallization occurred already during the cooling trajectory between 483 K and $T_c =$ 409 K [33].

In order to define the onset of crystallization, tangents were drawn along G'' in the nearly horizontal regime and in the regime of maximum changes, respectively (Fig. 7). The intercept t_{ind} is defined as a measure for the time elapsed before crystallization sets in, known as induction time.

The flow-induced experiments were performed under constant shearing time of 60 s and at a constant induction time of 0 s. It is clearly seen that

Table 2
Crystallization parameters

Polymer	Ref.	ΔH_0 ($\times 10^8$ J/m^3)	T_m (K)	T (K)	n	K_n [K(J/m^3)^n]	ρ (kg/m^3)	M_e^{26}	T_d (s)	τ (s)
pp	[24]	1.4	481	394	1	2.0×10^{11}	970	4623	1.86	0.66
pp	[25]	1.4	443	413	1	6.0×10^{10}	970	4623	10.1	
iPP	[27]	1.4	467	413	1	9.0×10^{10}	970	4623	40	10
iPP	This	1.4	483	409	1	2.1×10^{11}	905	4623	10	10

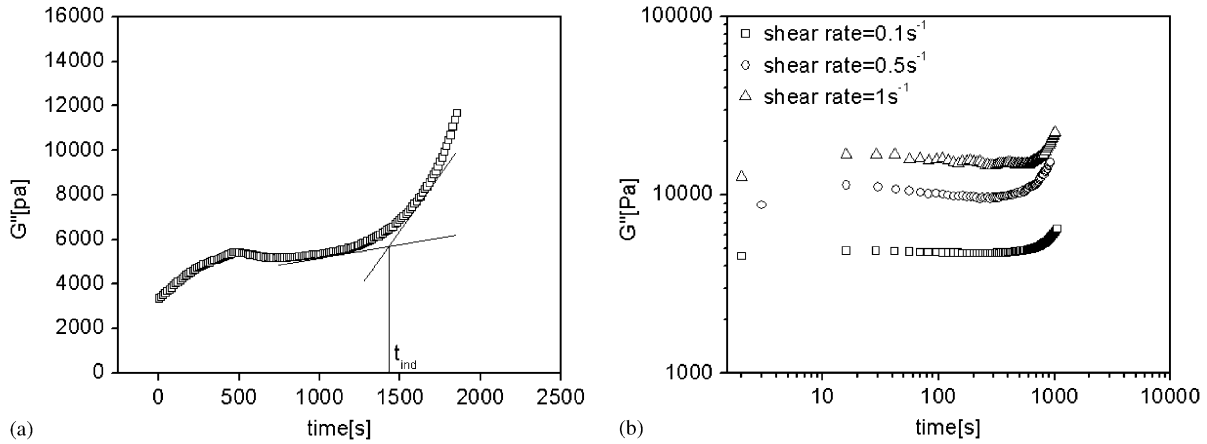

Fig. 7. Effect of shear rate on development of loss modulus at constant shearing time of ($t_s = 60$ s) and induction time ($t_0 = 0$) for iPP at isothermal $T_c = 409$ K. (a) Quiescent crystallization. (b) Under shear. Tangent is drawn to determine t_{ind} (solid lines).

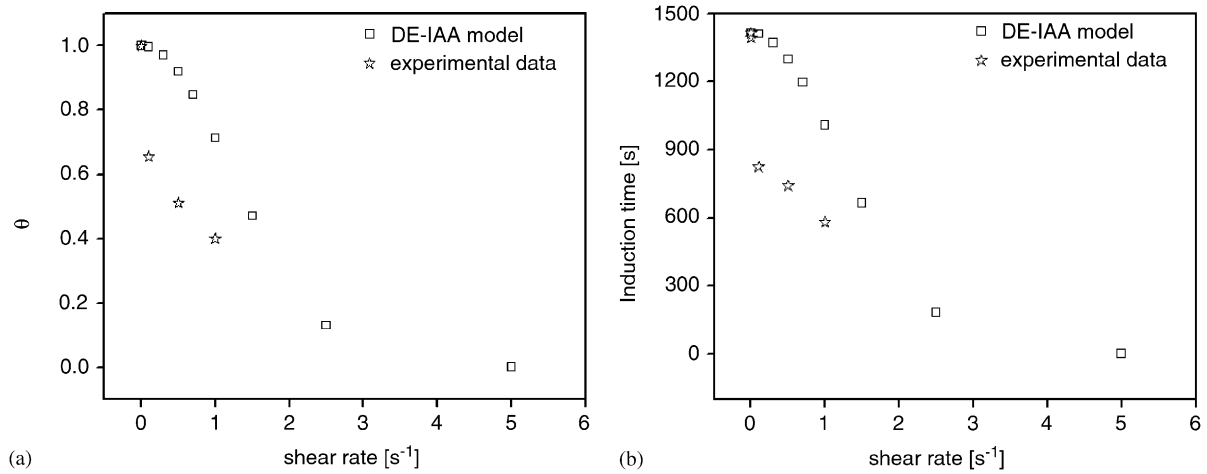

Fig. 8. Dimensionless induction time and induction time as a function of shear rate for iPP at isothermal $T_c = 409$ K. (a) Dimensionless induction time. (b) Induction time.

flow substantially accelerates the crystallization process.

The comparison of the model with rheology experiments is shown in Fig. 8. The comparison shows good agreement between model and experiment at low shear rates of the order of 0.001 s^{-1}. As the shear rate is increased, there is a substantial deviation observed between our experimental data and the results of the DE-IAA model. This observation shows once again the cumulative effect of the shear rate and the shearing

time. It also shows the importance of a critical dwell time as introduced by Devaux [38].

5. Conclusions

The effect of flow on the global crystallization kinetics of iPP has been studied by systematically varying the parameters affecting the kinetics. The influence of these parameters is evaluated with emphasis on the early stages of crystallization behavior of iPP (Table 2). Particularly the early formation of small crystallite domains during cooling of the sheared melt alters the crystallization behavior substantially, not only affecting the morphology but also the overall kinetics. These observations show the importance of a sensible combination of shear rate, shearing time and time of induction of shear. Both, the microscopic and the rheological results support this observation. The application of the DE-IAA model also confirms the deviation from the normal crystallization behavior and shows its validity at low shearing times.

References

[1] J.A. Odell, D.T. Grubb, A. Keller, Polym. Sci. 14 (1970) 617.
[2] A. Keller, H.W. Kolnaar, Flow induced orientation and structure formation, in: H.E.M. Meijer (Ed.), Processing of Polymers, vol.18, VCH, New York, 1997, pp. 189–268.
[3] G. Strobl, Eur. Phys. J. E: Soft Mater. 3 (2000) 165.
[4] B. Lotz, Eur. Phys. J. E: Soft Mater. 3 (2000) 185.
[5] M. Mutukumar, Eur. Phys. J. E: Soft Mater. 3 (2000) 199.
[6] Z. Menick, D.R. Fithmun, Polym. Sci.: Polym. Phys. 11 (1973) 973.
[7] D.R. Fithmun, Z. Menick, Polym. Sci.: Polym. Phys. 11 (1973) 951.
[8] A. Peterlin, Colloid. Polym. Sci. (1987) 265–357.
[9] R.K. Gupta, K.F. Auyeung, J. Appl. Polym. Sci. 34 (1987) 2469.
[10] Y. Ulcer, M. Calemak, Polym. Sci. (1987) 265.
[11] M. Fujiyama, T. Wakino, Y. Kawasaki, J. Appl. Polym. Sci. (1988) 29–35.
[12] M. Fujiyama, T. Wakino, J. Appl. Polym. Sci. 43 (1991) 57.
[13] R.R. Lagasse, B. Maxwell, Polym. Eng. Sci. 16 (1976) 189.
[14] P.G. Andersen, S.H. Carr, Polym. Eng. Sci. 18 (1978) 215.
[15] C. Tribout, B. Monasse, J.M. Haudin, Colloid. Polym. Sci. 274 (1996) 197.
[16] C.H. Sherwood, F.P. Price, R.S. Stein, J. Polym. Sci. Polym. Sympos. 63 (1978) 77.
[17] B. Monasse, J. Mater. Sci. 30 (1995) 5002.
[18] A. Keller, M.J. Machin, J. Macromol. Sci. Phys. B 1 (1967) 41.
[19] S. Coppola, N. Grizzuti, P.L. Maffettone, Macromolecules 34 (2001) 5030.
[20] M.J. Avrami, Chem. Phys. 7 (1939) 1103.
[21] H.G. Zachmann, H.A. Stuart, Makromol. Chem. 49 (1960) 131.
[22] D. Raabe, Acta Materialia 52 (2004) 2653.
[23] D. Raabe, in: B. Bacroix, J.H. Driver, R. Le Gall, Cl. Maurice, R. Penelle, H. Réglé, L. Tabourot, (Eds.), Proceedings of the Second Joint International Conference on Recrystallization and Grain Growth, France, Trans Tech Publications, Materials Science Forum 603, 2004, pp. 467–470.
[24] S.F. Doi Edwards, The theory of Polymers Dynamics, Clarendon Press, Oxford Press, England, 1986.
[25] H.C. Ottinger, A.N. Beris, J. Chem. Phys. 110 (1999) 6593.
[26] R.R. Lagasse, B. Maxwell, Polym. Eng. Sci. 16 (1976) 189.
[27] J. Neih, L. Lee, Polym. Eng. Sci. 38 (1998) 1121.
[28] J.I. Lauritzen, J.D. Hoffman, J. Rev. Natl. Bur. Stand. 64A (1960) 73.
[29] S. Acierno, Private communication (2004).
[30] G. Kumaraswamy, J.A. Kornfield, F.J. Yeh, B.S. Hsiao, Macromolecules 35 (2002) 1762.
[31] M. Seki, D.W. Thurman, J.P. Oberhauser, J.A. Kornfied, Macromolecules 35 (2002) 2583.
[32] H. Janeschitz-Kriegl, E. Ratajski, H. Wippel, Colloid. Polym. Sci. 277 (1999) 217.
[33] S. Vleeshouwers, H.E.H. Meijer, A rheological study of shear induced crystallization, Rheol. Acta 35 (1996) 391.
[34] N. Devaux, Ph.D. Thesis, CIT Kuleuven, 2003.
[35] C. Dupley, B. Monasse, J.M. Hauudin, J.L. Costa, J. Mater. Sci. 35 (2000) 1762.
[36] G.C. Alfonso, A. Ziabicki, Colloid. Polym. Sci. 273 (1995) 317.
[37] R. Kolb, C. Wutz, N. Stribeck, G. Von Krosigk, C. Riekel, Polymer 42 (2001) 5257.
[38] N. Deavaux, B. Monasse, J.M. Haudin, P. Moldenaers, J. Vermant, Rheol. Acta 43 (2004) 210.
[39] J.M. Schultz, E.W. Fischer, H.G. Zachmann, J. Polym. Phys. Edn. 18 (1980) 239.
[40] E. Kocher, R. Fulchiron, Polymer 43 (2002) 6931.
[41] G. Eder, Fundamentals of structure formation in crystallizing polymers, in: K. Hatada, T. Kitayama, O. Vogl (Eds.), Macromolecular Design of Polymeric Materials, Marcel Dekker, New York, 1997, p. 761.
[42] R.H. Somani, L. Yang, B.S. Hsiao, Physica A 304 (2002) 145.
[43] R.H. Somani, L. Yang, L. Zhu, B.S. Hsiao, Polymer 46 (2005) 8587.
[44] T. Okada, H. Saito, T. Inoue, Macromolecules 25 (1992) 1908.
[45] N.V. Pogodina, S.K. Siddique, J.W. Van Egmond, H.H. Winter, Macromoelcules 32 (1999) 1167.